Understanding the antibacterial efficacy of additively manufactured copper-added 316L stainless steel

Michael B. Myers and Amit Bandyopadhyay*

W. M. Keck Biomedical Materials Research Lab

School of Mechanical and Materials Engineering

Washington State University, Pullman, WA 99164-2920, USA

*Corresponding author email: amitband@wsu.edu

Abstract

In response to the growing demand for advanced materials with inherent infection resistance, this research investigates the properties of 316L stainless steel with copper, produced through laser-directed energy deposition additive manufacturing. The study focuses on three compositions: pure 316L, 316L with 3 wt.% Cu, and 316L with 5 wt.% Cu. Compressive strength measurements and Vickers hardness tests were conducted to assess mechanical properties, while microstructural characterization and X-ray diffraction analysis provided insights into the material's physical properties. This research extends beyond physical and mechanical properties by exploring the on-contact antibacterial efficacy against *Staphylococcus aureus* and *Pseudomonas aeruginosa* up to 72 h. The addition of Cu reduced the ability of bacterial colonization of both strains on the metal surface. The findings of this investigation have the potential to benefit the biomedical and medical device manufacturing sectors, contributing to both structural and bio-functional properties of materials.

Keywords: 316L stainless steel; Directed energy deposition (DED); Additive manufacturing; Copper; infection control.

1. Introduction

Approximately 2 million fracture fixation devices are inserted annually in the United States, amounting to a market value of $3.6 billion.[1,2] These devices, such as screws, rods, and plates, are implanted within the body to facilitate healing and strengthen injured limbs. However, there is a significant risk of infection associated with the implantation of a foreign device, affecting as high as 30% of cases.[3] Implants can potentially introduce foreign bacteria to the surgical site, leading to complications such as delayed healing and the need for additional surgeries. Revision surgeries can be traumatic and costly for patients, as reimplanted devices have an infection rate that is several times higher than that of first-time implants.[1] Furthermore, the median cost for treatment of a surgical site infection is approximately $108,000.[4] Therefore, reducing the risk of infection is crucial for improving patient outcomes.

Metallic materials are frequently favored over ceramics and polymers for implant production due to their superior strength and fatigue resistance.[5] Implant materials experience not just static loading but also dynamic loads associated with joints and movement. Additionally, implant materials must be biocompatible, resistant to corrosion, and not introduce toxicity to the body. While materials such as titanium or cobalt-chromium alloys are some of the many options available, 316L stainless steel (SS) is commonly used in implants and fracture management devices due to its high strength, excellent corrosion resistance, and good biocompatibility while remaining relatively low cost.[6] These properties are crucial for a material that will be subjected to fluctuating loads while exposed to the biological environment of the human body. However, 316L does not possess inherent antibacterial properties.[7] Patients are often required to take antibiotic medication to address concerns of post-surgery infection, but this provides only temporary protection. Moreover, bacterial strains can become antibiotic-resistant, rendering the patient vulnerable to infection. As a result, there is a need for an alloy with similar mechanical properties to 316L while incorporating antibacterial features.

Copper (Cu) has long been recognized for its antibacterial properties, as it can disrupt bacterial cell membranes and inhibit the growth of various pathogens.[7–12] Due to its antibacterial effect, Cu is used in critical surfaces found in drinking water distribution and hospital applications.[13] Yet, its antibacterial effect is joined with concerns of toxicity. Other antibacterial metals, like Ag, have also been studied for toxicity when used for implant applications. Increased

Ag levels can be found in bodily fluids, though most effects are seen in local tissue surrounding the implant site.[14] Therefore, toxicity may depend on the alloy's dose and the implant site's sensitivity. Similarly, Cu toxicity may depend on several factors. A Cu ion concentration of 46 μg/ml is highly toxic to fibroblasts in mice, while 2 mg/L may reach harmful levels in humans.[15,16]

While the exact method of Cu contact killing is still not fully understood, this has not withheld the element from being used as an antibacterial material.[8] Even though toxicity may not be boiled down to a simple alloying percentage, previous work has suggested Cu loadings up to 3% to be non-toxic while still providing an antibacterial effect.[9] In contrast, separate studies suggest that a 316L-5Cu composition has a lower tensile strength than 316L, but a 316L-3.5Cu alloy has improved hardness over 316L after undergoing an aging treatment.[17,7] 316L-Cu alloys have the potential to significantly improve the function of biomedical implants by becoming intrinsically resistant to bacterial colonization. However, a challenge lies in achieving the right balance of Cu to enhance antibacterial effects without compromising the alloy's mechanical integrity or resulting in toxicity to the body.

Additive manufacturing (AM) is a manufacturing method with ever-expanding popularity due to its various advantages over traditional production methods. Among other benefits, AM enables the production of intricate designs, easily customizable parts, and small batch production.[18] These properties make AM an ideal method for producing biomedical devices. AM enables varying part sizes and geometry, allowing implants to be custom fit to a patient. The process also makes producing custom and small numbers of parts financially accessible because it does not rely on fixed tooling. Additionally, the AM process is well-suited for producing custom alloy compositions due to its particle form feedstock. Within the family of AM processes, laser-directed energy deposition (L-DED) is well-fitted for biomedical device manufacturing due to its higher material deposition rate over other methods and precise control over alloy composition in small volumes.[19,20] DED can also produce functionally graded materials for optimized performance, such as hard surfaces for wear resistance and tough cores for load-bearing capacity. Therefore, AM and DED are attractive processes for producing metallic biomedical devices. While previous work has explored the mechanical and antibacterial properties of 316L-Cu, there is limited insight into this alloy as produced by AM.

This research aims to test the mechanical and antibacterial properties of 316L, 316L-3Cu (SS-3Cu), and 316L-5Cu (SS-5Cu) for implants and fracture management devices. It is hypothesized that adding Cu into a 316L matrix will provide inherent antibacterial properties and similar mechanical performance to 316L when produced through laser DED. Mechanical properties were evaluated by compressive loading and hardness measurements, along with microstructure characterization. Antibacterial performance was measured with 316L as the control against *Staphylococcus aureus* (*S. aureus*) and *Pseudomonas aeruginosa* (*P. aeruginosa*) to measure the effect of Cu addition against two common implant-related bacterial strains.[1,3]

2. Materials and methods

2.1. Sample preparation

The raw materials used in this study consisted of 316L SS powder (Höganäs, Sweden) with particle sizes ranging from 20 to 55 μm and Cu powder (GKN Hoeganaes, Cinnaminson, NJ) with particle sizes ranging from 15 to 53 μm. Although the L-DED system used in this study supports a larger powder size distribution, this particle size range was chosen to balance several properties. Finer particles were found to reduce powder flowability due to agglomeration, while coarser particles lead to increased porosity and surface roughness on the final part. Two alloy compositions were prepared: SS-3Cu and SS-5Cu. These powders were tumble mixed in batches of 250 g and mixed at 160 rpm for 2 h with no pause time to reach a uniform particle size distribution. The powder mixtures were contained in 500 mL jars with an air atmosphere. All samples were fabricated using a FormAlloy laser DED system (Spring Valley, CA). The processing parameters consisted of 350 W laser power and 575 mm/min scan speed for contour and infill paths, with 0.3 mm layer thickness, 0.78 mm hatch spacing, and 20° C build plate temperature. Powder feed settings included 0.5 rpm powder feeder disc rate, 9 L/min carrier gas flow rate, and 13 L/min shield gas flow rate. It was observed that the Cu addition did not affect the processing parameters, as the same settings were used for all three compositions. To minimize oxidation, the printing environment was carefully maintained with an oxygen concentration below 20 ppm, and the chamber was filled with argon gas. The samples were

designed as vertical cylinders with a diameter of 9 mm and a height of 18 mm and were printed onto a 316L substrate.

2.2. Microstructure and phase analysis

Samples for microstructural analysis were produced by sectioning the cylindrical specimens longitudinally, exposing a vertical cross-section. These sections were then mounted in phenolic resin and ground using silicon carbide (SiC) pads in sequential order of increasing grit size from 320 to 1200. The samples were subsequently polished with alumina suspensions of 1 µm, 0.3 µm, and 0.05 µm particle size, using deionized (DI) water as the medium. Etching was performed following ASTM E407 – 23.[21] The etching solution comprised 10 mL HNO_3, 35 mL HCl, and 30 mL H_20, with 60 s immersion, followed by a rinse in water and air drying. Microstructure imaging was done using a digital microscope (VHX-970F, Keyence, Itasca, IL). The grain size was calculated using the average grain intercept (AGI) method, where the number of grain intercepts was divided by the line length. Phase analysis was performed using X-ray diffraction (XRD) with a Rigaku MiniFlex 600 diffractometer (Rigaku, Japan). The samples were scanned using Cu-K α radiation (1.54 Å at 40 kV and 20 mA) with a 2θ theta range of 25° – 100° and a scan rate of 5° per min. Energy dispersive spectroscopy (EDS) was conducted using a field emission scanning electron microscope (FE-SEM, Sirion) for five minutes. For EDS analysis, samples were cut in the XY plane, which refers to the horizontal plane parallel to the build platform and perpendicular to the build direction (Z-axis), to map elemental distribution across the print plane.

2.3. Compression and hardness testing

Cylindrical compression test specimens were machined using a computer numerical control (CNC) mill (770MX, Tormach, Madison, WI) equipped with a lathe attachment. The diameter of the specimens was milled to 7.5 mm, and the length was faced to 15 mm, resulting in a length-to-diameter (L/D) ratio of 2. Compression testing was performed following ASTM E9 – 19.[22] The tests were conducted using a universal test machine (600DX, Instron, Norwood, MA) at a constant crosshead displacement rate of 0.1 mm/min. These tests were terminated once the

specimens reached 4% engineering strain, with n = 3 tests performed for each composition. Hardness testing was conducted according to ASTM E92 – 23[23], using a Micro Vickers Hardness Tester (Phase II Plus, Upper Saddle River, NJ). Hardness samples were prepared in the same manner as the microstructure samples. Vickers hardness measurements were taken at 0.5 mm intervals, starting from the base of the sample and extending up to a height of 5 mm. A load of 1.961 N (HV 0.2) was applied, with a dwell time of 15 s.

2.4. *In vitro* bacterial studies

The antibacterial efficacy of Cu addition into 316L was evaluated *in vitro* against *S. aureus* and *P. aeruginosa* bacterial strains at 24, 48, and 72 h. The AM-produced cylindrical specimens were sliced into 1 mm thick sections using a low-speed diamond saw, then mounted and ground with SiC pads up to 1200 grit. These samples were subsequently cleaned via ultrasonication and sterilized by autoclaving at 121 °C for 1 h. *S. aureus* and *P. aeruginosa* (Carolina Biological, Burlington, NC) were rehydrated with rehydration media and incubated at 37 °C for 24 h to reactivate. Serial dilutions of the bacterial cultures were performed to achieve a concentration corresponding to the 0.5 McFarland standard, equivalent to 1.5×10^8 colony-forming units (CFU)/mL, as confirmed by optical absorbance measurements within a range of 0.08-0.1 at a wavelength of 625 nm. For antibacterial testing, the sterilized samples were placed into 24-well plates, with 10^6 CFU applied on the surface of each sample, followed by 1 mL of nutrient broth. The plates were then incubated at 37 °C until the specified time points. At each time point, the nutrient broth was carefully removed and replaced with a fixative solution (2% paraformaldehyde/ 2% glutaraldehyde in 0.1 M phosphate-buffered saline [PBS]) overnight. After removal of the fixative solution, the samples underwent secondary fixation with 1% osmium tetroxide (OsO_4) overnight, followed by a rinse in DI water. The samples were then subjected to a serial dehydration process using increasing concentrations of ethanol (30%, 50%, 70%, 90%, and greatly with 100%). After dehydration, the samples were treated with hexamethyldisilane (HMDS) overnight. A gold coating layer was applied to the samples to facilitate the imaging of organic material via SEM. A minimum of n = 3 images were collected per time point and composition for bacterial colony quantification. The antibacterial efficacy of each material composition was determined by counting the number of bacterial colonies (N) on

the surface of the samples using an open-source object counting software (DotDotGoose).[24] Antibacterial efficacy, based on the control and treatment CFU counts at each time point, was calculated as follows:

$$R = \frac{N_{control} - N_{treatment}}{N_{control}} \times 100 \quad (1)$$

3. Results

3.1. Microstructure, EDS, and phase analysis

The microstructure of 316L consisted of distinct regions exhibiting both cellular and columnar dendritic solidification modes. The regions appeared to have a uniform structure, with clear boundaries between the two formations. **Fig. 1a** displays a low-magnification image of 316L, showing four printed layers, with a mix of cellular and columnar structures across the layers. The transition between these two formations is distinctly visible at higher magnification. The columnar dendrites are oriented along the heat flow direction, or normal to the top and bottom surface of each layer, and largely aligned in the vertical direction due to cooling provided by the substrate. **Fig. 1b** and **Fig. 1c** also reveal a similar mix of cellular and columnar dendrite structures, with no significant differences between these compositions and the 316L base material. Equiaxed structures for 316L, SS-3Cu, and SS-5Cu were measured with diameters of 5 ± 1 μm, finding that Cu addition did not change grain size significantly. All three compositions resulted in fully dense samples, except for minor gas entrapment defects. These defects, caused by trapped gas particles during the solidification of the melt pool, appeared as spherical voids of 30 μm or less.

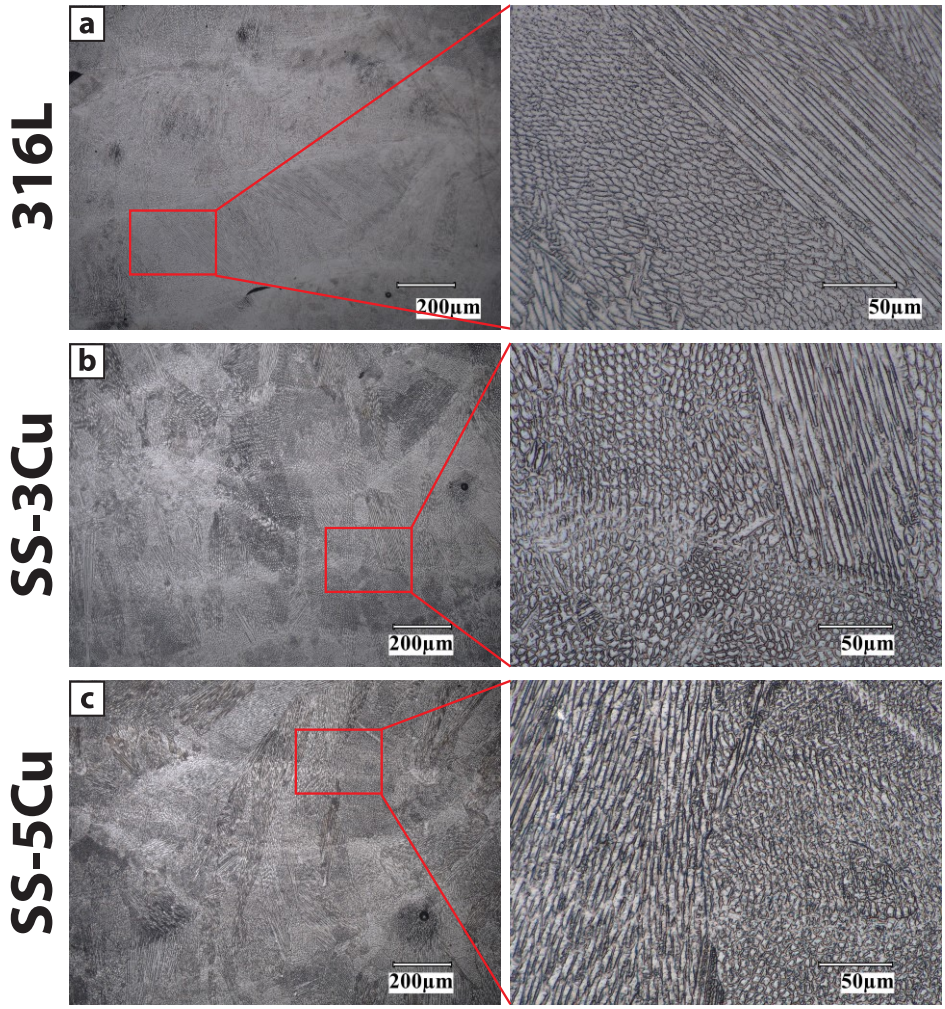

Figure 1: (a) 316L control composition displayed a mix of cellular and columnar structures visible in high magnification. (b, c) SS-3Cu and SS-5Cu showed microstructures similar to those of the control composition.

EDS was conducted to examine the Cu distribution within the 316L base composition. As seen in **Fig. 2**, Cu was uniformly distributed within 316L, suggesting the formation of a solid solution. Chromium and nickel, the main alloying elements of 316L[25], also appeared evenly distributed. Achieving a uniform Cu distribution is ideal for implant applications where a consistent antibacterial effect is desired across the surface of an implant. Since bacteria and other foreign materials typically contact the outer surface of an implant first upon entering the body, the surface properties play a critical role in determining the overall antibacterial efficacy.

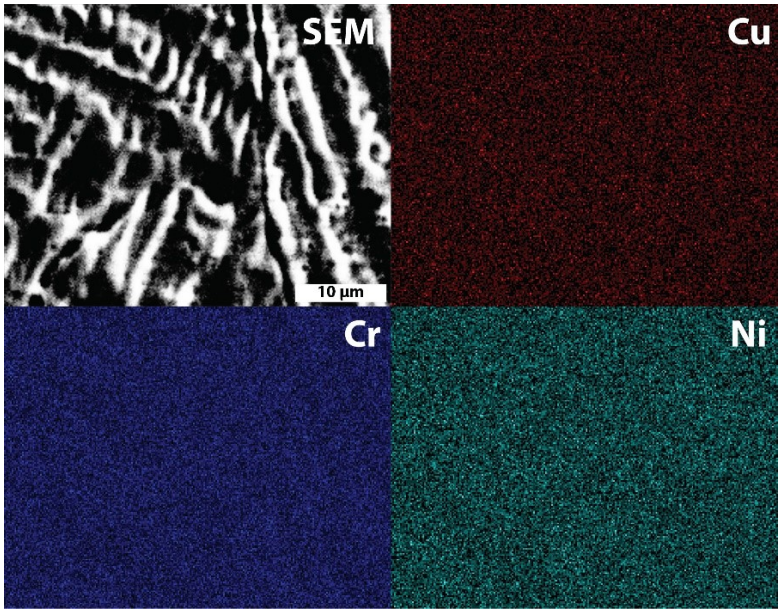

Figure 2: EDS mapping of the SS-5Cu surface revealed a homogenous copper, chromium, and nickel distribution.

XRD measurements were performed on all three compositions to identify the phases present, as shown in **Fig. 3**. The XRD pattern of 316L exhibited a primary characteristic peak at a 2θ value of 43.64°, corresponding to face-centered cubic (FCC) austenite in the (111) plane. Notably, the SS-3Cu and SS-5Cu compositions showed an increased intensity of the (111) peak relative to 316L, which can be attributed to adding Cu. However, the intensities of the secondary peaks [(200), (220), and (311)] remained essentially unchanged. This selective enhancement of the (111) peak suggests that Cu addition induces a preferential orientation of the grains. Additionally, SS-3Cu peaks exhibited a slight shift in the negative direction (~0.15°), which further increased in SS-5Cu (~0.22°). No martensitic phases were detected in the XRD patterns of 316L, and no new peaks were detected in SS-3Cu and SS-5Cu within the detection limit, suggesting that Cu addition did not lead to the formation of any new phases compared to the 316L scan pattern.

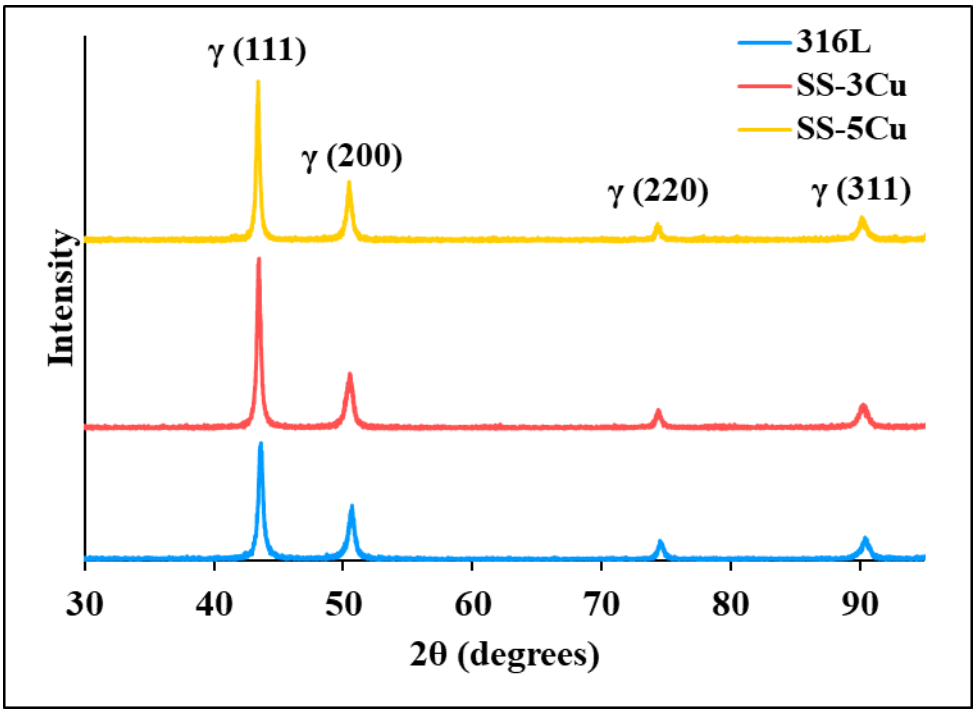

Figure 3: XRD patterns of 316L, SS-3Cu, and SS-5Cu. Cu addition in SS-3Cu and SS-5Cu resulted in an enlarged relative peak height at ~44°, corresponding to face-centered cubic austenite.

Table 1: XRD angle and peak intensity values of 316L, SS-3Cu, and SS-5Cu.

Peak No.	*hkl*	316L (2θ, Intensity a.u.)	SS-3Cu (2θ, Intensity a.u.)	SS-5Cu (2θ, Intensity a.u.)
1	(111)	43.64°, 313	43.49°, 455	43.42°, 429
2	(200)	50.69°, 146	50.51°, 149	50.47°, 161
3	(220)	74.52°, 52	74.38°, 52	74.35°, 49
4	(311)	90.41°, 61	90.27°, 66	90.13°, 67

3.2. Compression and hardness testing

The compressive behavior of all three compositions was found to be similar, as illustrated by the representative stress-strain curves shown in **Fig. 4a**. The yield stress values for 316L, SS-3Cu, and SS-5Cu were 334 ± 9 MPa, 329 ± 12 MPa, and 317 ± 1 MPa, respectively. Cu addition appeared to have minimal impact on the yield stress. This is advantageous for implant

applications, where 316L is commonly used, as adding Cu would not result in a substantial change in strength. **Fig. 4b** presents the Vickers hardness measurements taken along the build direction, starting from the bottom of the sample. The hardness values of 316L, SS-3Cu, and SS-5Cu were 209 ± 12, 183 ± 9, and 186 ± 10 HV 0.2, respectively. Although both Cu compositions exhibited lower hardness than 316L, no significant difference was observed between SS-3Cu and SS-5Cu. Moreover, hardness measurements for all three compositions showed no significant variation across the height of the samples, suggesting a consistent hardness distribution along the build direction.

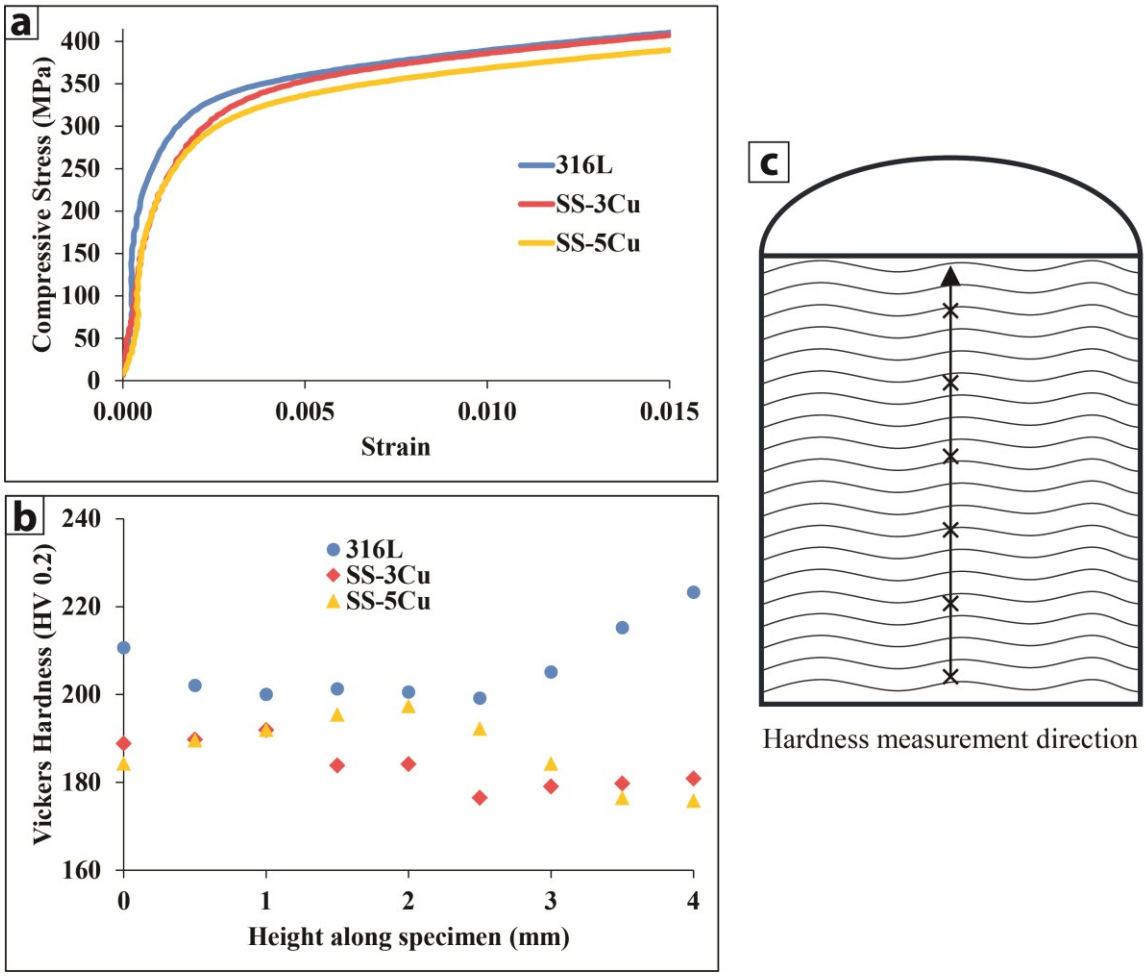

Figure 4: (a) Representative stress-strain curves for all three compositions show similar behavior under uniaxial compression loading. (b) Vickers hardness measurements showed a slight

reduction with Cu presence, plotted as a three-point moving average. (c) Illustration of hardness measurement locations on a cylinder cross-section.

3.3. *In vitro S. aureus* bacterial study

Cu is known for its antibacterial properties and was expected to reduce bacterial surface colonization when incorporated into 316L.[7,10] Gram-positive *S. aureus* was tested on the metal surfaces at 24, 48, and 72 h, simulating the time points immediately following a surgical procedure. As shown in **Fig. 5a1-3**, the 316L control surfaces were heavily colonized by *S. aureus*. In contrast, Cu addition reduced bacterial colonization on the treated surfaces. The SS-3Cu samples demonstrated lower CFU counts at all time points (**Fig. 5b1-3**), while the SS-5Cu samples exhibited even more significant reductions in bacterial growth (**Fig. 5c1-3**). Quantification of visible CFU is summarized in **Fig. 5d**, while the normalized bacterial viability is presented in **Fig. 5e**. On SS-3Cu surfaces, *S. aureus* colonization decreased from 30% at 24 h to 25% at 48 h and 18% at 72 h. This corresponds to a 5% reduction between 24 and 48 h and a 7% reduction between 48 and 72 h. SS-5Cu surfaces displayed superior antibacterial performance, with remaining CFU values of 19% at 24 h, 14% at 48 h, and 12% at 72 h., reflecting 5% and 2% reductions between respective time points. The antibacterial efficacy followed a logarithmic trend, with the most significant reduction occurring within the first 24 h. While the rate of antibacterial performance slowed at later time points, incremental improvements in efficacy were observed. Notably, the inset image in **Fig. 5c1** highlights an *S. aureus* cell exhibiting cell wall rupture and exposed cytoplasm, providing visual evidence of the antibacterial effect of Cu addition and its potential use in infection-resistant materials.

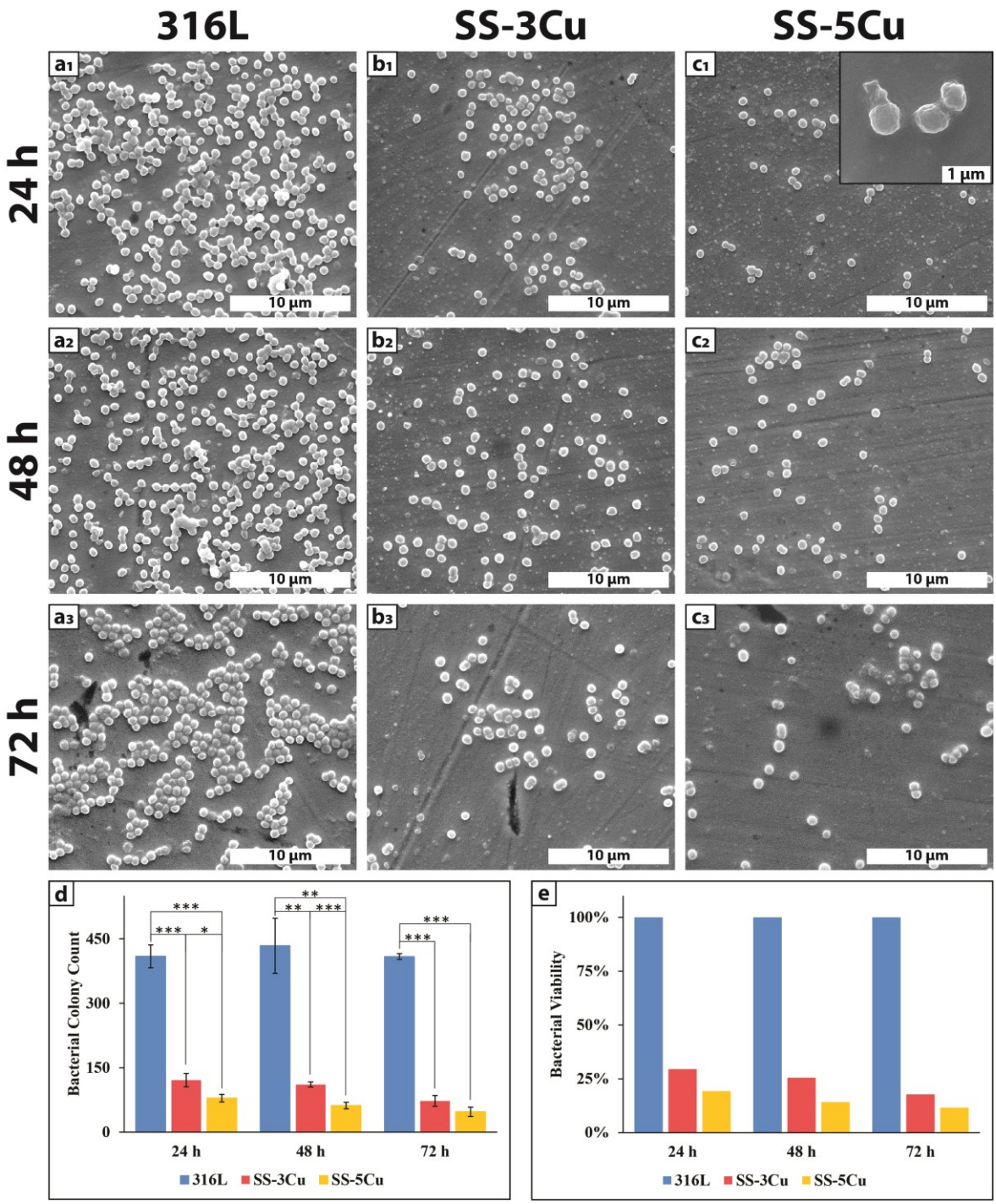

Figure 5: SEM imaging and quantification of visible *S. aureus* CFU. (a1, a2, a3) 316L control shows significantly higher CFU count than (b1, b2, b3) SS-3Cu and (c1, c2, c3) SS-5Cu across all time points. (d) CFU quantification of SEM images with n = 3 per condition. Statistically significant values are marked as * $p < 0.05$, ** $p < 0.01$, *** $p < 0.001$. (e) Normalized bacterial viability for each time point.

3.4. *In vitro P. aeruginosa* bacterial study

Antibacterial performance was further evaluated at 24 and 48 h against *P. aeruginosa*, a gram-negative bacteria. The 316L control surfaces displayed a pronounced increase in bacterial colony count over time, with CFU counts rising significantly from 422 ± 46 at 24 h to 1819 ± 226 CFU at 48 h, as seen in **Fig. 6a1-a2**. This increase demonstrates an environment conducive to bacterial proliferation on the 316L surface. In contrast, the SS-3Cu surface showed substantially reduced bacterial viability, with CFU counts of 92 ± 25 and 114 ± 40 at 24 and 48 h, respectively, corresponding to 22% and 6% of the control bacterial colonies, as shown in **Fig. 6b1-b2**. A similar trend was observed on SS-5Cu surfaces, which demonstrated even higher antibacterial efficacy, with CFU counts of 63 ± 12 and 57 ± 10 at the same time points, representing 15% and 3% bacterial viability, respectively, as shown in **Fig. 6c1-c2**. While the 316L samples demonstrated a significant increase in CFU between time points, the Cu-loaded samples effectively suppressed bacterial growth, with minimal changes in CFU counts from 24 to 48 h. This inhibition of bacterial proliferation highlights the role of Cu as an antimicrobial agent.

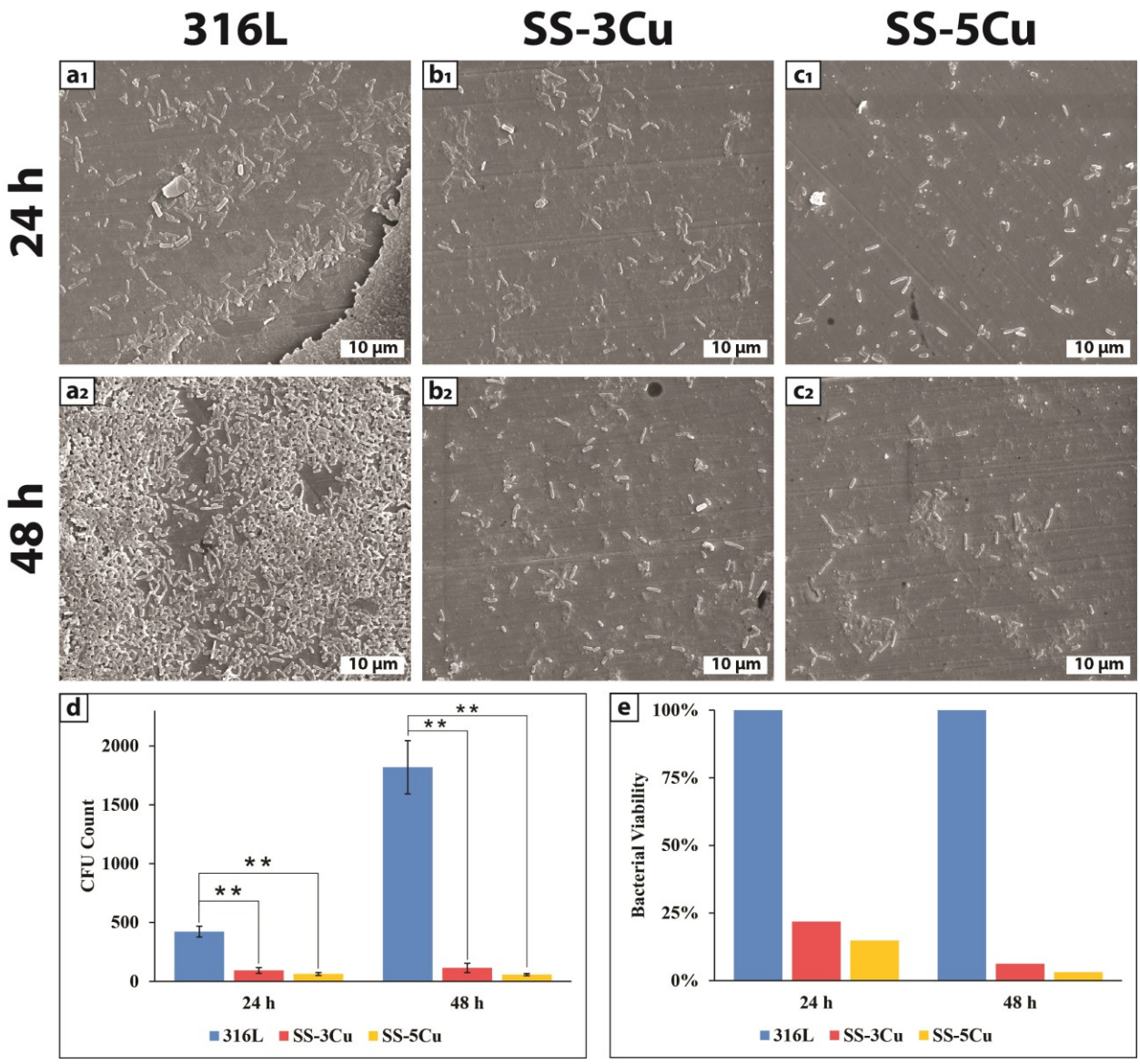

Figure 6: SEM imaging and agar plate quantification of *P. aeruginosa* activity. (a1, a2) 316L control surface with increasing CFU count over time. (b1, b2) SS-3Cu and (c1, c2) SS-5Cu show a significant reduction in bacteria with respect to the control composition. (d) CFU quantification of SEM images with n = 3 per condition. Statistically significant values are marked as * $p < 0.05$, ** $p < 0.01$, *** $p < 0.001$. (e) Normalized bacterial viability for each time point.

4. Discussion

316L SS is widely used in the medical industry for its strength and corrosion resistance while maintaining good biocompatibility. These properties are critical for implant and fracture management applications, where the environment of the human body presents a dynamic situation ideally suited for corrosion and infection. When alloyed with 316L, Cu has been shown to inhibit bacterial proliferation and holds promising potential for use in biomedical settings. This study aimed to measure the mechanical and antibacterial properties of 316L-Cu alloys produced through DED.

4.1. Microstructure and mechanical properties

Microstructural analysis revealed two distinct formations within 316L. Cellular and columnar dendritic solidification was observed in all three compositions, as shown in **Fig. 1**. Columnar formations result from the pronounced thermal gradient experienced during the DED process, with structures growing preferentially along the heat flow direction towards the chilled substrate. On the other hand, the growth of cellular structures can be attributed to the rapid solidification rate, moderate thermal gradients present within the melt pool, and lack of heat flow in the XY plane, all of which favor the development of cellular dendritic structures. In contrast, traditional manufacturing methods, such as cold-rolling, begin with equiaxed austenitic grains and transform into elongated martensitic structures due to the rolling process. Strain-induced martensite can be reversed into austenite through annealing, increasing its strength through grain size reduction and achieving finer grain sizes than the original austenite.[26]

The incorporation of Cu did not appear to significantly alter the microstructure of 316L, which is consistent with previous findings in other studies of Cu-alloyed 316L produced through traditional manufacturing methods.[7] Cu addition into 316L has also been achieved through powder bed fusion (PBF), another popular AM process, and exhibited similar Cu dissolution in a 316L matrix.[27] Although this study found similarly sized equiaxed structures for all three compositions, it has been reported that higher Cu loadings may lead to increased temperature gradients due to the higher thermal conductivity of Cu over 316L (385 vs. ~20 W/m·K), causing grain refinement.[28]

EDS mapping was conducted to determine the elemental distribution across sample surfaces. As shown in **Fig. 2**, the analysis confirmed the uniform distribution of Cu with no preferential concentrations in the grain structure. 316L, composed of approximately 18% Cr and 14% Ni[25], appeared to form a solid solution with Cu addition, as shown in previous works.[27,28] A homogenous Cu distribution ensures consistent mechanical and antibacterial properties. Phase analysis was performed using XRD (**Fig. 3**), which revealed an exclusive FCC austenite phase within the detection limit across all compositions, with diffraction peaks corresponding to the (111), (200), (220), and (311) planes. The slight shift in peak positions for SS-3Cu and SS-5Cu has also been reported in similar work involving 316L-Cu alloys.[27–30] A possible cause for this shift could be residual stresses caused by substituting Cu atoms into the Fe lattice, leading to a change in lattice parameters due to the difference in atomic radius of the two elements.

Compressive stress-strain behavior (**Fig. 4**) showed that all compositions had similar compressive strength values. A slight reduction in yield strength was observed for SS-5Cu (317 ± 1 MPa) compared to 316L (334 ± 9 MPa) and SS-3Cu (329 ± 12 MPa). Similarly, a minor reduction in hardness was measured in the Cu compositions (183 ± 9 and 186 ± 10 HV 0.2 for SS-3Cu and SS-5Cu, respectively) compared to 316L (209 ± 12 HV 0.2). Previous studies have reported similar reductions in strength and hardness with Cu addition in samples produced by LPBF.[17] This trend has also been recorded in alloys produced through forging[7], though this same study also demonstrated a notable increase in strength and hardness after applying a heat treatment cycle. Conversely, increases in strength and hardness have been reported directly after production via PBF.[27,29] This property variation could be credited to varying amounts of Cu and differing manufacturing methods, leading to differences in the microstructure. While the magnitude of property variation from the base 316L is minor, this lack of consensus highlights the variability of material properties in AM-produced alloys and their dependence on processing parameters.

4.2. Antibacterial properties

While Cu is known to have antibacterial properties, its exact method of killing bacteria remains a topic of ongoing research, with no single definite consensus. One accepted theory of contact killing involves the ability of released Cu ions to degrade the cell membrane, leading to leakage of cellular contents and eventual cell death. An alternative hypothesis suggests that Cu

ions penetrate the membrane and generate reactive oxygen species (ROS), which causes oxidative stress that damages cellular contents, including DNA.[8,31] Both theories converge on the same outcome: cell death resulting from membrane damage due to surface contact with Cu.

Although Cu alloying has great antibacterial potential, more established and trusted infection prevention methods are widely employed. Antibiotic medication may be administered post-surgery to address infection risks, but this protection is temporary. Similarly, antibacterial coatings can be applied to implants, but their efficacy may diminish as the coatings degrade. In contrast, Cu addition provides an inherent antibacterial effect that may last for the entire lifespan of an implant, preventing bacterial colonization and biofilm formation for extended periods after implantation. However, antibacterial implants alone may not address infection risks on surfaces not in direct contact with the device, such as adjacent tissue near the surgical site. Therefore, 316L-Cu alloys could be used in conjunction with antibiotics or coatings to provide both short- and long-term antibacterial protection.

This study measured antibacterial performance against *S. aureus* (**Fig. 5**) and *P. aeruginosa* (**Fig. 6**). The results demonstrated that both Cu compositions exhibited significant antibacterial efficacy compared to 316L. SS-5Cu showed greater effectiveness than SS-3Cu due to its higher Cu content, consistent with prior studies that report increased antibacterial efficacy with progressive Cu addition.[7–9,12] The growth of both *S. aureus* and *P. aeruginosa* was significantly inhibited in SS-3Cu and SS-5Cu samples, emphasizing the potential of these alloys for biomedical applications. These findings align with previous studies on 316L-Cu alloys produced using AM and conventional methods.[7,10,29]

5. Conclusions

This study investigated the microstructural, mechanical, and antibacterial properties of 316L SS with 3 wt.% and 5 wt.% Cu produced through powder-based Laser-DED. The following conclusions can be drawn from this study.

(a) The incorporation of Cu resulted in no significant change in the microstructure and appeared to form a homogenous distribution of Cu within the matrix, as confirmed by SEM, EDS, and XRD.

(b) Compressive strength and hardness values remained comparable to 316L despite these elemental modifications. A slight reduction in yield strength was observed for SS-5Cu (317 ± 1 MPa) compared to 316L (334 ± 9 MPa) and SS-3Cu (329 ± 12 MPa). Similarly, a minor reduction in hardness was measured in the Cu compositions (183 ± 9 and 186 ± 10 HV 0.2 for SS-3Cu and SS-5Cu, respectively) compared to 316L (209 ± 12 HV 0.2).

(c) Cu addition demonstrated significant antibacterial efficacy. SS-3Cu and SS-5Cu effectively inhibited the growth of *S. aureus* and *P. aeruginosa* across all time points, with efficacy increasing proportionally with the Cu content. After testing against *S. aureus*, the two compositions exhibited 18% and 12% bacterial viability at 72 h, respectively. More effectively, results for *P. aeruginosa* at 48 h indicate 6% and 3% bacteria viability. This highlights the potential of these alloys for use in biomedical environments, particularly in infection-prone applications such as fracture management devices.

The findings suggest that 316L with Cu addition offers a promising balance between mechanical performance and antibacterial functionality, making it a viable material for advanced biomedical devices.

6. Acknowledgments

The authors would like to acknowledge financial support from the National Science Foundation under Grant Number CMMI1934230 and the National Institute of Arthritis and Musculoskeletal and Skin Diseases of the National Institutes of Health under Award Number R01 AR078241 (PI: Bandyopadhyay). The content is solely the authors' responsibility and does not necessarily represent the National Institutes of Health's official views. The authors would also like to acknowledge experimental help from Aruntapan Dash and Nathaniel Zuckschwerdt.

7. Conflict of interest

The authors declare no conflict of interest.

8. Author contributions

Conceptualization: Amit Bandyopadhyay

Formal analysis: Michael B. Myers

Funding acquisition: Amit Bandyopadhyay

Investigation: Michael B. Myers

Project administration: Amit Bandyopadhyay

Supervision: Amit Bandyopadhyay

Writing – original draft: Michael B. Myers

Writing – review & editing: Amit Bandyopadhyay

9. Ethics approval and consent to participate

Not applicable.

10. Consent for publication

Not applicable.

11. Availability of data

Data is available upon request.

12. ORCID IDs

Michael B. Myers: https://orcid.org/0009-0005-4946-1048

Amit Bandyopadhyay: https://orcid.org/0000-0003-0992-5387

13. References

1. Darouiche RO. Device-Associated Infections: A Macroproblem that Starts with Microadherence. *Clin Infect Dis*. 2001;33(9):1567-1572. doi:10.1086/323130

2. *Orthopedic Trauma Devices Market Size, Share & COVID-19 Impact Analysis | United States | 2019-2025*. iData Research; 2019. Accessed November 25, 2024. https://idataresearch.com/product/trauma-devices-market-united-states/

3. Steinmetz S, Wernly D, Moerenhout K, Trampuz A, Borens O. Infection after fracture fixation. *EFORT Open Rev*. 2019;4(7):468-475. doi:10.1302/2058-5241.4.180093

4. Thakore RV, Greenberg SE, Shi H, et al. Surgical site infection in orthopedic trauma: A case–control study evaluating risk factors and cost. *J Clin Orthop Trauma*. 2015;6(4):220-226. doi:10.1016/j.jcot.2015.04.004

5. Kim T, See CW, Li X, Zhu D. Orthopedic implants and devices for bone fractures and defects: Past, present and perspective. *Eng Regen*. 2020;1:6-18. doi:10.1016/j.engreg.2020.05.003

6. DeVasConCellos P, Bose S, Beyenal H, Bandyopadhyay A, Zirkle LG. Antimicrobial particulate silver coatings on stainless steel implants for fracture management. *Mater Sci Eng C*. 2012;32(5):1112-1120. doi:10.1016/j.msec.2012.02.020

7. Xi T, Shahzad MB, Xu D, et al. Effect of copper addition on mechanical properties, corrosion resistance and antibacterial property of 316L stainless steel. *Mater Sci Eng C*. 2017;71:1079-1085. doi:10.1016/j.msec.2016.11.022

8. Vincent M, Duval R e., Hartemann P, Engels-Deutsch M. Contact killing and antimicrobial properties of copper. *J Appl Microbiol*. 2018;124(5):1032-1046. doi:10.1111/jam.13681

9. Bandyopadhyay A, Mitra I, Ciliveri S, et al. Additively manufactured Ti–Ta–Cu alloys for the next-generation load-bearing implants. *Int J Extreme Manuf*. 2023;6(1):015503. doi:10.1088/2631-7990/ad07e7

10. Zhuang Y, Zhang S, Yang K, Ren L, Dai K. Antibacterial activity of copper-bearing 316L stainless steel for the prevention of implant-related infection. *J Biomed Mater Res B Appl Biomater*. 2020;108(2):484-495. doi:10.1002/jbm.b.34405

11. Dash A, Bose S, Bandyopadhyay A. Additively manufactured 17–4 PH stainless steels for fracture management devices. *Virtual Phys Prototyp*. 2024;19(1):e2397698. doi:10.1080/17452759.2024.2397698

12. Chen KK, Chao CY, Chen JH, Wu JH, Chang YH, Du JK. Effect of Low Copper Addition to As-Forged 304 Stainless Steel for Dental Applications. *Metals*. 2021;11(1):43. doi:10.3390/met11010043

13. Vincent M, Hartemann P, Engels-Deutsch M. Antimicrobial applications of copper. *Int J Hyg Environ Health*. 2016;219(7, Part A):585-591. doi:10.1016/j.ijheh.2016.06.003

14. Hadrup N, Sharma AK, Jacobsen NR, Loeschner K. Distribution, metabolism, excretion, and toxicity of implanted silver: a review. *Drug Chem Toxicol*. 2022;45(5):2388-2397. doi:10.1080/01480545.2021.1950167

15. Cao B, Zheng Y, Xi T, et al. Concentration-dependent cytotoxicity of copper ions on mouse fibroblasts in vitro: effects of copper ion release from TCu380A vs TCu220C intra-uterine devices. *Biomed Microdevices*. 2012;14(4):709-720. doi:10.1007/s10544-012-9651-x

16. Badhe RV, Akinfosile O, Bijukumar D, Barba M, Mathew MT. Systemic toxicity eliciting metal ion levels from metallic implants and orthopedic devices – A mini review. *Toxicol Lett*. 2021;350:213-224. doi:10.1016/j.toxlet.2021.07.004

17. Foadian F, Kremer R, Post M, Taghizadeh Tabrizi A, Aghajani H. Investigation of In-Situ Low Copper Alloying of 316L Using the Powder Bed Fusion Process. *Solids*. 2023;4(3):156-165. doi:10.3390/solids4030010

18. Bandyopadhyay A, Bose S. *Additive Manufacturing*. 2nd Edition. CRC Press; 2019. doi:10.1201/9780429466236

19. Guide for Additive Manufacturing — Design — Directed Energy Deposition. doi:10.1520/F3413-19E01

20. Bandyopadhyay A, Traxel KD, Lang M, Juhasz M, Eliaz N, Bose S. Alloy design via additive manufacturing: Advantages, challenges, applications and perspectives. *Mater Today*. 2022;52:207-224. doi:10.1016/j.mattod.2021.11.026

21. Standard Practice for Microetching Metals and Alloys. doi:10.1520/E0407-23

22. Standard Test Methods of Compression Testing of Metallic Materials at Room Temperature. doi:10.1520/E0009-19

23. Standard Test Methods for Vickers Hardness and Knoop Hardness of Metallic Materials. doi:10.1520/E0092-23

24. Ersts PJ. DotDotGoose. Accessed November 25, 2024. https://biodiversityinformatics.amnh.org/open_source/dotdotgoose/

25. Standard Specification for Wrought 18Chromium-14Nickel-2.5Molybdenum Stainless Steel Bar and Wire for Surgical Implants (UNS S31673). doi:10.1520/F0138-19

26. Kheiri S, Mirzadeh H, Naghizadeh M. Tailoring the microstructure and mechanical properties of AISI 316L austenitic stainless steel via cold rolling and reversion annealing. *Mater Sci Eng A*. 2019;759:90-96. doi:10.1016/j.msea.2019.05.028

27. Behjat A, Shamanian M, Iuliano L, Saboori A. Laser powder bed fusion in situ alloying of AISI 316L-2.5%Cu alloy: microstructure and mechanical properties evolution. *Prog Addit Manuf*. Published online January 24, 2024. doi:10.1007/s40964-023-00557-x

28. Liu Y, Yang J, Yang H, et al. Cu-bearing 316L stainless steel coatings produced by laser melting deposition: Microstructure and corrosion behavior in simulated body fluids. *Surf Coat Technol*. 2021;428:127868. doi:10.1016/j.surfcoat.2021.127868

29. Behjat A, Shamanian M, Sadeghi F, Iuliano L, Saboori A. Additive manufacturing of a novel in-situ alloyed AISI316L-Cu stainless steel: Microstructure and antibacterial properties. *Mater Lett*. 2024;355:135363. doi:10.1016/j.matlet.2023.135363

30. Płatek P, Sienkiewicz J, Janiszewski J, Jiang F. Investigations on Mechanical Properties of Lattice Structures with Different Values of Relative Density Made from 316L by Selective Laser Melting (SLM). *Materials*. 2020;13:2204. doi:10.3390/ma13092204

31. Grass G, Rensing C, Solioz M. Metallic Copper as an Antimicrobial Surface. *Appl Environ Microbiol*. 2011;77(5):1541-1547. doi:10.1128/AEM.02766-10